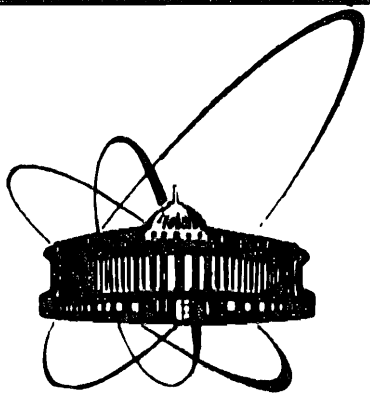

объединенный
институт
ядерных
исследований
дубна

E1-87-549

A HIGH STATISTICS MEASUREMENT OF THE NUCLEON STRUCTURE FUNCTION $F_2(x, Q^2)$ FROM DEEP INELASTIC MUON-CARBON SCATTERING AT HIGH Q^2

BCDMS Collaboration

Submitted to "Physics Letters B"

1987

A.C.Benvenuti, D.Bollini, G.Bruni, T.Camporesi[1], G.Heiman[1], L. Monari, F.L.Navarria
Dipartimento di Fisica dell Universita and INFN, Bologna, Italy

A.Argento[2], M.Bozzo[3], R.Brun, J.Cvach[4], H.Gennow[5], L.Piemontese[6], D.Schinzel
CERN, Geneva, Switzerland

D.Yu.Bardin, N.G.Fadeev, I.A.Golutvin, Yu.T.Kiryushin, V.S.Kisselev, V.G.Krivokhizhin, V.V.Kukhtin, W.Lohmann[7], P.Reimer, I.A.Savin, G.I.Smirnov, J.Strachota, G.Sultanov[8], P.Todorov, A.G.Volodko
Joint Institute for Nuclear Research, Dubna

D.Jamnik[9], R.Kopp[10], U.Meyer-Berkhout, A.Staude, K.-M.Teichert, R.Tirler[11], R.Voss, Č.Zupančič
Sektion Physik der Universität, München, Federal Republic of Germany[12]

J.Feltesse, A.Milsztajn, A.Ouraou, J.F.Renardy, P.Rich-Hennion, Y.Sacquin, G.Smadja, P.Verrecchia, M.Virchaux
DPhPE, CEN Saclya, France

[1]Now at CERN, Geneva, Switzerland.
[2]Now at Digital Equipment, Torino, Italy.
[3]Now at INFN, Genova, Italy.
[4]On leave from Institute of Physics, CSAV, Prague, Czechoslovakia.
[5]Now at University of Stockholm, Stockholm, Sweden.
[6]Now at INFN, Trieste, Italy.
[7]On leave from the Institute für Hochenergiephysik der AdW der DDR, Berlin-Zeuthen, GDR.
[8]Now at the Institute of Nuclear Research and Nuclear Energy, Bulgarian Academy of Science, Sofia, Bulgaria.
[9]On leave from E.Kardelj University and the J.Stefan Institute, Ljubljana, Yugoslavia.
[10]Now at Siemens AG, Münich, FRG
[11]now at DPhPE, CEN Saclya, France.
[12]Funded in part by the German Federal Minister for Research and Technology (BMFT) under contract number 054MU12P6.

Deep inelastic scattering of leptons is firmly established as a fundamental tool to investigate the quark-parton structure of the nucleon. In the one-photon exchange approximation, the deep inelastic muon-nucleon cross section can be written as

$$\frac{d^2\sigma}{dQ^2dx} = \frac{4\pi\alpha^2}{Q^4 x}\cdot\left[1-y-\frac{Q^2}{4E^2}+\frac{y^2E^2+Q^2}{2E^2[R(x,Q^2)+1]}\right]\cdot F_2(x,Q^2), \quad (1)$$

where E is the energy of the incident beam, Q^2 the squared four-momentum transfer between the muon and the hadronic system, and x and y are the Bjorken scaling variables. $F_2(x,Q^2)$ is the nucleon structure function and $R = \sigma_L/\sigma_T$ is the ratio of absorption cross sections for virtual photons of longitudinal and transverse polarization.

In this paper, we present new results on the nucleon structure functions $F_2(x,Q^2)$ and $R(x,Q^2)$ measured in deep inelastic scattering of muons on a carbon target. The data were collected with a high-luminosity spectrometer at the CERN SPS muon beam. The experimental apparatus is described in detail elsewhere /1/. It consists of a 50 m long segmented toroidal iron magnet which is magnetized close to saturation and surrounds a 40 m long target. The target and the iron absorb the hadronic shower close to the interaction point and the surviving scattered muon is focused towards the spectrometer axis. The toroids are instrumented with scintillation trigger counters and multiwire proportional chambers. Four hodoscopes along the spectrometer axis detect the incoming muons and measure their trajectories. The momentum of the incident muons is measured with a spectrometer consisting of an air-gap magnet and another four scintillator hodoscopes upstream of the apparatus. Preliminary results obtained with this set-up have been reported earlier /2/.

The analysis presented here is based on $1.5\cdot10^6$ reconstructed events recorded with muon beams of 120, 200 and 280 GeV energy. Beam polarities, kinematic ranges and data samples after all cuts are summarised in Table I.

Table 1: The data sample

Beam energy (GeV)	Beam signs	Q^2 range (GeV^2)	x range	Number of events
120	μ^+/μ^-	25-115	0.25-0.8	280 000
200	μ^+/μ^-	42-200	0.25-0.8	280 000
280	μ^+	58-280	0.25-0.8	120 000

The 120 and 200 GeV data represent a subset of a data sample used earlier to search for weak-electromagnetic interference effects in deep inelastic muon scattering[3]. In view of the high statistical accuracy of these data, a large effort was invested in calibrating the apparatus and in monitoring its performance, in order to reduce systematic errors to a similar level. As the most important systematic limitation of the experiment is the energy calibration of the incident and scattered lepton, special emphasis was put on calibrating the magnetic field in the iron toroids where it is not measurable directly. A map of the magnetic excitation $\vec{H}$ was measured in the thin air gaps between individual discs of the iron toroids[1] and extrapolated into the iron. It was converted into magnetic induction $\vec{B}$ using accurately measured permeability curves for a large number of iron samples. The magnetic flux through the iron toroids, i.e. the overall normalization of the field map, and its azimuthal dependence were verified with induction loops wound around various segments of the magnet. From the accuracy of these measurements and from other independent cross-cheks, we estimate an uncertainty of $1 \cdot 10^{-3}$ on the point-to-point variation of the field map and an uncertainty of $2 \cdot 10^{-3}$ on its overall calibration. The air gap magnet of the beam momentum spectrometer[1] was calibrated to an accuracy ranging from $1.5 \cdot 10^{-3}$ at 120 GeV beam energy to better than $1 \cdot 10^{-3}$ at 280 GeV.

To calibrate the luminosity of the experiment, the incident beam of $\approx 2 \cdot 10^7$ μ/sec intensity was counted with a fast plastic scintillator hodoscope[1] using two different methods:

1. The signals from the central 48 scintillators of this hodoscope which define the "beam" trigger of the experiment are counted individually. A small correction (1-2%) is applied for electronic dead-time losses. The individual signals are then added and a 20-30% correction is applied for double counting due to geometrical overlap of the scintillators and small electromagnetic showers propagating in the hodoscope. This correction, albeit large, is reliably determined from special runs with low beam intensity.

2. The signals of the same 48 scintillators are ORed electronically and counted with scalers with fixed dead-times. To calculate the dead-time corrections of typically 15%, the distribution of the instantaneous beam intensity was monitored with time-to-digital converters.

The results obtained by these two methods agree to $\approx 0.2\%$ for the 200 GeV and 280 GeV data. For the 120 GeV data, only method 2 could be applied due to a malfunctioning of the electronics used to monitor the beam intensity for method 1.

The data were analyzed using a detailed Monte-Carlo simulation of the experiment which takes into account

- the phase space of the incoming beam;
- efficiencies and resolution properties of all detectors in the apparatus;
- multiple scattering and energy loss of both incident and scattered muons[4], simulating the stochastic nature of the energy losses;
- additional detector hits from δ rays generated along the muon track and from hadronic shower punch-through close to the interaction vertex.

For each of the three beam energies, $3.5 \cdot 10^6$ events were generated and processed through exactly the same chain of reconstruction programs as the experimental data. From the reconstructed Monte-Carlo events, fine-grain acceptance matrices in Q^2 and x which include all effects of spectrometer resolution are calculated to convert the experimental distributions into cross section. The geometrical acceptance is typically 75% and is rather flat in the kinematic region $Q^2/Q^2_{max} > 0.2$, $x > 0.3$ ($Q^2_{max} = 2ME$ where M is the nucleon mass). Data points where the acceptance is less than 40% or varies strongly over the corresponding bin are not used in the analysis. The magnetic field calibration and the description of the momentum resolution of the spectrometer by the Monte-Carlo simulation were verified in a series of special runs where beams of known momenta ranging from 50 to 280 GeV were deflected directly into the spectrometer iron. The systematic uncertainty on the measured structure function from spectrometer resolution is smaller than the calibration uncertainties.

To extract the one-photon exchange cross section from the measured data, corrections must be applied for higher order processes. The radiative corrections used in this analysis are described in detail in refs.[5] and include

- lepton current processes up to order α^4,
- vacuum polarization by leptons and quarks,
- hadron current processes of order α^3,
- effects of weak-electromagnetic γ-Z^0 interference[3].

The error on $F_2(x,Q^2)$ from uncertainties on these corrections is estimated to be smaller than 1%.

The unfolding of the spectrometer resolution and the radiative corrections require an a priori knowledge of the nucleon structure function which was therefore calculated with an iterative procedure. The final results are insensitive to the initial parametrization of $F_2(x, Q^2)$.

The comparison of cross sections measured at different beam energies allows to determine R and, in addition, provides a powerful cross-check of systematic errors. The deep inelastic cross section (eq. (1)) depends on R mainly in the region of large $y = \nu/E$ which is populated mostly by low x and high Q^2 events. In contrast, errors on the relative normalization of the data sets are independent of any kinematic variable and a scale error on the momentum measurement of incident or scattered muons affects mainly the region of small y, i.e. events at large x and small Q^2. Effects on the F_2 determination from these three different sources are therefore only weakly correlated and can be studied separately.

The structure function at 200 and 280 GeV beam energy are found to be in very good agreement, whereas the data points at 120 GeV are 2.5% lower everywhere in the kinematic region of overlap. Considering the aforementioned problem with the flux monitoring for these data, they were multiplied by 1.025 for the subsequent analysis. We assume normalization uncertainties of $\pm$ 1.0% of both the 120 and 280 GeV data relative to the 200 GeV data. The absolute normalization uncertainty of the combined data is estimated to be smaller than 3%.

We then study the mutual agreement of the three data sets under variation of the magnetic field calibration of the spectrometer. The χ^2 of the three $F_2(x,Q^2)$ with respect to each other exhibits a clear minimum when an overall factor $f_B = 1.0013 \pm 0.0008$ is applied to the field map, indicating that the calibration described above is indeed correct to $\approx 10^{-3}$. We chose to increase the field by a factor of 1.0013 and assign a systematic error of $\Delta B/B = 1.5 \cdot 10^{-3}$.

The structure functions at the three beam energies, after the renormalization of the 120 GeV data and with the final calibration of the magnetic field, assuming R = 0, are given in Tables 4-6 and are shown in Fig.1. ΔF_2 is the statistical error. The systematic errors are given as multiplicative factors to be applied to $F_2(x,Q^2)$; f_r, f_b, f_s and f_d are the uncertainties due to spectrometer resolution, beam momentum calibration, spectrometer magnetic field calibration and detector inefficiencies, respectively. The normalization uncertainties discussed in the text are not shown in the Table. The factor f_R indicates the variation of F_2 when R = 0.02 is assumed instead of R = 0. $R = \sigma_L/\sigma_T$ was determined with the same χ^2 method that was used for the magnetic field adjustment. The agreement among the three data sets is optimized separately in each bin of x but assuming R to be independent of Q^2 in the range 40 GeV$^2 \leq Q^2 \leq$ 200 GeV^2. This is consistent

with QCD calculations which predict only a weak (logarithmic) variation of R with Q^2 /6/,

$$R_{QCD}(x,Q^2) = \frac{F_L(x,Q^2)}{(1+4M^2x^2/Q^2)\cdot F_2(x,Q^2) - F_L(x,Q^2)}, \qquad (2)$$

where

$$F_L(x,Q^2) = \frac{\alpha_s(Q^2)}{2\pi}\cdot x^2 \int_x^1 \left[\frac{8}{3}F_2(z,Q^2) + \frac{40}{9}\left(1-\frac{x}{z}\right) z\,G(z,Q^2)\right]\cdot \frac{dz}{z^3} \qquad (3)$$

is the longitudinal structure function, $xG(x,Q^2)$ is the gluon momentum distribution and $\alpha_s(Q^2)$ is the running coupling constant of QCD. In the kinematic range of this measurement, R_{QCD} is almost insensitive to the shape of $xG(x,Q^2)$ which is assumed to be $xG(x)=4.5(1-x)^8$ at Q_o^2=25 GeV^2 and to the QCD mass scale parameter which is taken to be Λ =200 MeV. The result is shown in Table 2 and Fig.2 and is compatible both with R=0 and with the perturbative QCD prediction. We find a mean value of R= 0.015 $\pm$ $\pm$ 0.013 (stat.)$\pm$ 0.026 (syst.) in the range $0.25 \leq x \leq 0.7$ at an average Q^2=60 GeV^2. The systematic errors are dominated by the uncertainty on the relative cross section normalizations.

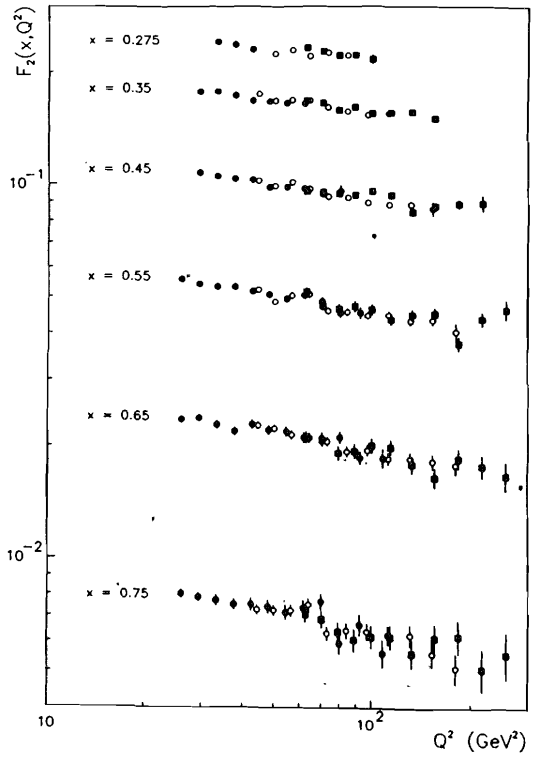

Fig.1. The nucleon structure function $F_2(x,Q^2)$ measured at the three beam energies 120 GeV (closed circles), 200 GeV (open circles), and 280 GeV(squares). The 120 GeV data were multiplied by a factor 1.025 to adjust the relative normalization of the three data sets. Only statistical errors are shown.

The final $F_2(x,Q^2)$ from the combined data sets using $R = R_{QCD}$ is shown in Fig.3. A parametrization of $F_2(x,Q^2)$ is given in Table 3. No errors on the parameters are given since they are strongly correlated. This parametrization should not be used outside the kinematic range of the data (cf. Table 1). The data exhibit clear deviations from Bjorken scaling. A detailed comparison of these scaling violations to QCD predictions is presented in a separate paper[9].

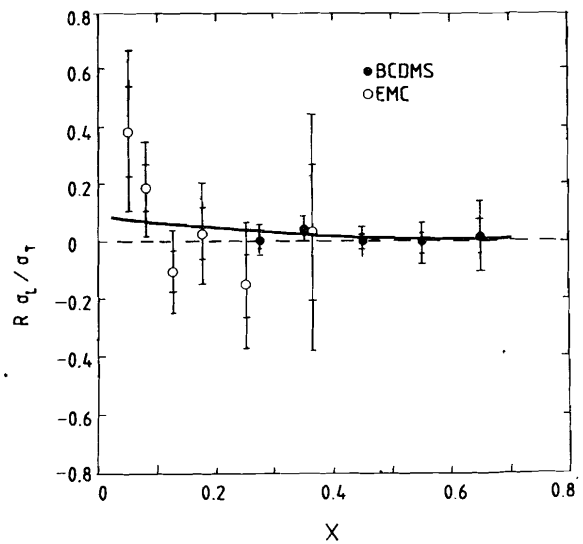

Fig.2. $R = \sigma_L/\sigma_T$ as a function of x. Also shown is the measurement by the EMC collaboration on an iron target[7]. Inner error bars are statistical errors only, outer error bars are statistical and systematic errors added lineary. The solid line represents the QCD prediction for Λ = 200 MeV.

Table 2: Results for $R = \sigma_L/\sigma_T$

x	$\langle Q^2 \rangle$ (GeV²)	R	statist. error	syst. error
0.275	60	0.004	0.028	0.020
0.35	60	0.041	0.020	0.024
0.45	60	−0.002	0.023	0.028
0.55	65	−0.009	0.037	0.034
0.65	70	0.015	0.060	0.059
all x	60	0.015	0.013	0.026

Results on $F_2(x,Q^2)$ from deep inelastic muon scattering on iron targets have been presented earlier by the BFP[8] and EMC[7] collaborations. We find a significantly steeper decrease of $F_2(x)$ with x than has been measured by the EMC(Fig.4), a trend opposite to what is expected from nuclear effects in deep inelastic scattering[10]. The

BFP data show an x dependence which is compatible with ours but are ≈ 4% lower in the overall normalization.

Table 3: Parametrization of $F_2(x,Q^2)$

$F_2(x,Q^2) = (1-x)^a \cdot (b + cx + dx^2 + ex^3) \cdot (Q^2)^{(f+gx)}$

a = 2.5693	b = 0.2739	c = 3.0437
d = −5.5172	e = 2.5790	f = −0.0303
g = −0.2185		

$x^2/DOF = 180/159$

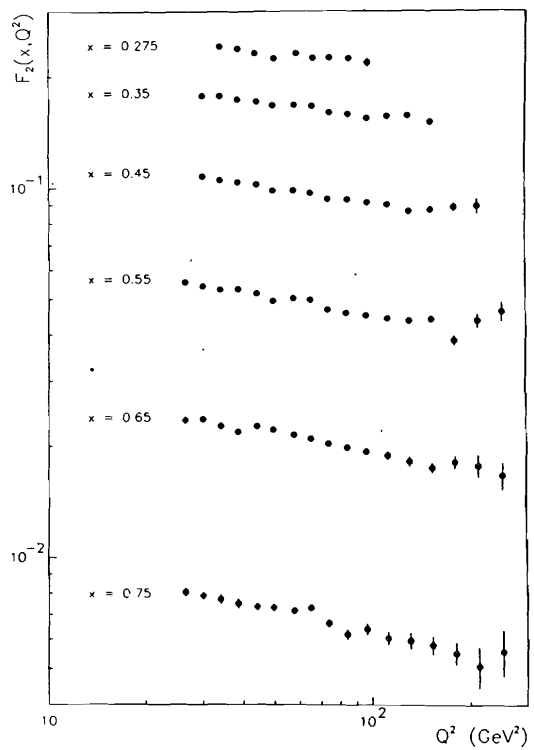

Fig.3. The structure function $F_2(x,Q^2)$ using $R = R_{QCD}$ for all beam energies combined. Only statistical errors are shown.

In conclusion, we have presented a high statistics measurement of the nucleon structure function $F_2(x,Q^2)$ from deep inelastic muon-carbon scattering at high Q^2 ($Q^2 \geq 25$ GeV²). Careful calibration of the experimental apparatus has allowed to reduce systematic uncertain-

ties to a level close to the statistical accuracy of the data. $R = \sigma_L/\sigma_T$ is found to be compatible, within small errors, both with zero and with the QCD prediction in the kinematic range $0.25 \leq x \leq 0.7$.

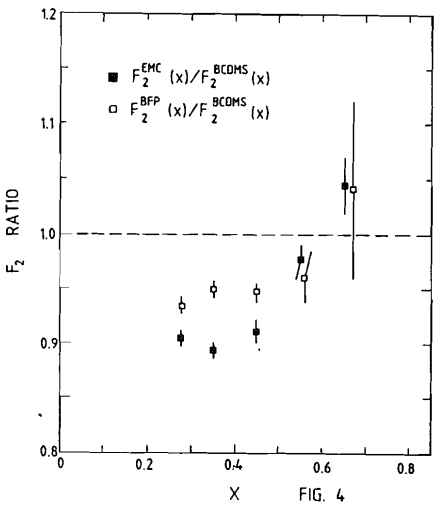

FIG. 4

Fig.4. The ratio of $F_2(x)$ measured in this experiment over $F_2(x)$ from the EMC/7/ and BFP/8/ collaborations. In each x bin, the ratio is determined in the Q^2 region of overlap between the respective data sets. Only statistical errors are shown.

Table 4: $F_2(x,Q^2)$ at 120 GeV beam energy

Average beam energy at the interaction vertex: $<E>$ = 113.6 GeV.

x	Q^2	F_2	ΔF_2	f_r	f_b	f_s	f_d	f_R
0.275	34.00	0.24038	0.00322	1.006	0.998	1.001	0.988	1.006
	38.50	0.23645	0.00320	1.003	0.998	1.001	0.988	1.008
	43.50	0.22955	0.00376	1.005	0.998	1.002	0.987	1.010
0.35	30.00	0.17676	0.00171	1.008	0.998	1.003	0.989	1.002
	34.00	0.17713	0.00192	1.001	0.998	1.003	0.990	1.003
	38.50	0.17294	0.00184	1.000	0.998	1.003	0.990	1.004
	43.50	0.16718	0.00183	1.003	0.998	1.003	0.991	1.006
	49.00	0.16643	0.00187	1.002	0.998	1.003	0.990	1.008
	55.50	0.16497	0.00218	1.002	0.998	1.003	0.989	1.010
	63.00	0.16449	0.00349	1.004	0.998	1.003	0.987	1.014
0.45	30.00	0.10740	0.00129	1.005	1.001	1.009	0.990	1.001
	34.00	0.10491	0.00152	0.998	1.000	1.008	0.991	1.002
	38.50	0.10339	0.00144	0.999	1.000	1.007	0.992	1.002
	43.50	0.10264	0.00143	1.002	0.999	1.007	0.993	1.003
	49.00	0.09790	0.00141	1.000	0.999	1.006	0.993	1.004
	55.50	0.09797	0.00142	1.002	0.999	1.006	0.993	1.006
	63.00	0.09718	0.00150	1.002	0.999	1.005	0.993	1.008
	71.50	0.09394	0.00181	1.003	0.998	1.005	0.991	1.010
	81.50	0.09545	0.00358	1.003	0.998	1.005	0.988	1.014

0.55	26.50	0.05560	0.00100	1.016	1.008	1.022	0.988	1.001
	30.00	0.05410	0.00083	1.013	1.006	1.019	0.990	1.001
	34.00	0.05311	0.00101	1.004	1.005	1.017	0.992	1.001
	38.50	0.05313	0.00099	1.005	1.004	1.016	0.993	1.001
	43.50	0.05162	0.00100	1.006	1.003	1.014	0.994	1.002
	49.00	0.05069	0.00102	1.002	1.002	1.013	0.995	1.003
	55.50	0.04931	0.00099	1.003	1.001	1.011	0.995	1.004
	63.00	0.05040	0.00108	1.002	1.000	1.010	0.995	1.005
	71.50	0.04856	0.00114	1.003	1.000	1.009	0.995	1.006
	81.50	0.04512	0.00119	1.004	0.999	1.009	0.994	1.009
	94.00	0.04516	0.00159	1.005	0.999	1.008	0.991	1.012
0.65	26.50	0.02345	0.00049	1.057	1.020	1.044	0.989	1.000
	30.00	0.02360	0.00043	1.039	1.017	1.039	0.991	1.001
	34.00	0.02265	0.00055	1.024	1.014	1.034	0.992	1.001
	38.50	0.02180	0.00054	1.026	1.011	1.030	0.994	1.001
	43.50	0.02271	0.00060	1.021	1.009	1.027	0.995	1.001
	49.00	0.02198	0.00062	1.013	1.007	1.024	0.996	1.002
	55.50	0.02178	0.00064	1.014	1.006	1.022	0.996	1.002
	63.00	0.02101	0.00066	1.011	1.004	1.019	0.997	1.003
	71.50	0.02089	0.00073	1.009	1.003	1.017	0.997	1.004
	81.50	0.02099	0.00077	1.009	1.001	1.015	0.996	1.006
	94.00	0.01852	0.00077	1.009	1.000	1.014	0.995	1.008
	110.50	0.01851	0.00106	1.015	0.999	1.012	0.992	1.012
0.75	26.50	0.00802	0.00021	1.123	1.043	1.084	0.989	1.000
	30.00	0.00785	0.00020	1.105	1.037	1.074	0.991	1.000
	34.00	0.00769	0.00024	1.093	1.031	1.065	0.992	1.001
	38.50	0.00750	0.00024	1.090	1.026	1.058	0.994	1.001
	43.50	0.00749	0.00028	1.082	1.021	1.051	0.995	1.001
	49.00	0.00739	0.00030	1.068	1.018	1.045	0.996	1.001
	55.50	0.00714	0.00031	1.065	1.014	1.040	0.997	1.002
	63.00	0.00735	0.00034	1.053	1.011	1.035	0.997	1.002
	71.50	0.00763	0.00039	1.044	1.008	1.031	0.997	1.003
	81.50	0.00591	0.00037	1.039	1.006	1.027	0.997	1.004
	94.00	0.00663	0.00043	1.030	1.004	1.024	0.997	1.006
	110.50	0.00558	0.00047	1.030	1.002	1.021	0.996	1.009

Table 5: $F_2(x,Q^2)$ at 200 GeV beam energy

Average beam energy at the interaction vertex: $<E>$ = 191.7 GeV.

x	Q^2	F_2	ΔF_2	f_r	f_b	f_s	f_d	f_R
0.275	50.00	0.22312	0.00259	1.006	0.998	1.001	0.991	1.004
	56.50	0.22822	0.00304	1.000	0.998	1.001	0.992	1.005
	64.00	0.22026	0.00297	1.002	0.998	1.001	0.992	1.007
	73.00	0.22493	0.00280	1.006	0.998	1.002	0.991	1.010
	84.00	0.22121	0.00358	1.004	0.998	1.002	0.988	1.014
0.35	44.50	0.17420	0.00179	1.004	0.998	1.003	0.990	1.002
	50.00	0.16699	0.00171	1.002	0.998	1.003	0.992	1.002
	56.50	0.16802	0.00199	0.998	0.998	1.003	0.994	1.003
	64.00	0.16757	0.00190	1.001	0.998	1.003	0.994	1.004
	73.00	0.16039	0.00168	1.002	0.998	1.003	0.995	1.006
	84.00	0.15639	0.00177	1.002	0.998	1.003	0.995	1.008
	97.00	0.15305	0.00191	1.005	0.998	1.003	0.993	1.011
	112.50	0.15472	0.00284	1.004	0.998	1.003	0.988	1.016

0.45	44.50	0.10180	0.00136	1.003	1.002	1.010	0.991	1.001
	50.00	0.09867	0.00135	1.001	1.001	1.009	0.993	1.001
	56.50	0.10099	0.00159	0.997	1.000	1.008	0.995	1.002
	64.00	0.09698	0.00148	1.000	1.000	1.007	0.996	1.002
	73.00	0.09232	0.00132	1.002	1.000	1.007	0.997	1.003
	84.00	0.09182	0.00138	1.000	0.999	1.006	0.997	1.004
	97.00	0.08897	0.00142	1.002	0.999	1.006	0.997	1.006
	112.50	0.08790	0.00152	1.002	0.998	1.005	0.997	1.009
	131.00	0.08791	0.00179	1.004	0.998	1.005	0.994	1.013
	153.00	0.08570	0.00357	1.005	0.998	1.005	0.987	1.018
0.55	44.50	0.05200	0.00092	1.012	1.008	1.022	0.992	1.001
	50.00	0.04835	0.00091	1.008	1.007	1.020	0.994	1.001
	56.50	0.05029	0.00106	1.004	1.005	1.018	0.996	1.001
	64.00	0.05079	0.00106	1.005	1.004	1.016	0.997	1.001
	73.00	0.04580	0.00093	1.004	1.003	1.014	0.997	1.002
	84.00	0.04542	0.00098	1.002	1.002	1.013	0.998	1.003
	97.00	0.04442	0.00102	1.003	1.001	1.011	0.998	1.004
	112.50	0.04460	0.00109	1.002	1.000	1.010	0.998	1.005
	131.00	0.04293	0.00116	1.004	0.999	1.009	0.998	1.008
	153.00	0.04311	0.00132	1.004	0.999	1.008	0.997	1.011
	180.00	0.04011	0.00207	1.006	0.998	1.007	0.990	1.016
0.65	44.50	0.02254	0.00049	1.044	1.020	1.044	0.992	1.000
	50.00	0.02214	0.00051	1.034	1.017	1.039	0.994	1.001
	56.50	0.02136	0.00059	1.026	1.014	1.035	0.996	1.001
	64.00	0.02096	0.00061	1.022	1.012	1.031	0.997	1.001
	73.00	0.02047	0.00058	1.019	1.009	1.027	0.998	1.001
	84.00	0.01920	0.00061	1.015	1.007	1.024	0.998	1.002
	97.00	0.01940	0.00066	1.012	1.005	1.021	0.999	1.003
	112.50	0.01843	0.00069	1.010	1.003	1.018	0.999	1.004
	131.00	0.01835	0.00075	1.008	1.002	1.016	0.999	1.005
	153.00	0.01807	0.00082	1.007	1.001	1.014	0.998	1.008
	180.00	0.01766	0.00098	1.008	0.999	1.013	0.997	1.011
0.75	44.50	0.00725	0.00021	1.138	1.043	1.084	0.992	1.000
	50.00	0.00723	0.00022	1.120	1.037	1.074	0.994	1.000
	56.50	0.00722	0.00026	1.105	1.031	1.065	0.996	1.001
	64.00	0.00749	0.00029	1.093	1.026	1.057	0.997	1.001
	73.00	0.00629	0.00026	1.081	1.021	1.050	0.998	1.001
	84.00	0.00639	0.00030	1.068	1.017	1.043	0.999	1.001
	97.00	0.00636	0.00033	1.059	1.013	1.037	0.999	1.002
	112.50	0.00624	0.00036	1.049	1.010	1.033	0.999	1.003
	131.00	0.00622	0.00040	1.040	1.007	1.028	0.999	1.004
	153.00	0.00556	0.00043	1.031	1.004	1.025	0.999	1.005
	180.00	0.00510	0.00047	1.028	1.002	1.021	0.999	1.008

Table 6: $F_2(x,Q^2)$ at 280 GeV beam energy

Average beam energy at the interaction vertex: $<E>$ = 270.5 GeV.

x	Q^2	F_2	ΔF_2	f_r	f_b	f_s	f_d	f_R
0.275	61.50	0.23244	0.00334	1.004	0.998	1.001	0.991	1.003
	69.00	0.22670	0.00335	1.002	0.998	1.001	0.993	1.004
	77.50	0.22105	0.00370	1.001	0.998	1.001	0.994	1.005
	87.00	0.22134	0.00396	1.001	0.998	1.001	0.995	1.007
	98.00	0.21643	0.00547	1.005	0.998	1.002	0.994	1.009

0.35	61.50	0.16744	0.00218	1.001	0.999	1.004	0.992	1.002
	69.00	0.16480	0.00218	1.002	0.998	1.003	0.994	1.002
	77.50	0.15743	0.00236	1.000	0.998	1.003	0.996	1.003
	87.00	0.16060	0.00254	1.000	0.998	1.003	0.997	1.004
	98.00	0.15462	0.00240	1.001	0.998	1.003	0.997	1.005
	112.00	0.15528	0.00242	1.001	0.998	1.003	0.997	1.007
	130.00	0.15593	0.00254	1.002	0.998	1.003	0.997	1.010
	152.50	0.14995	0.00304	1.004	0.998	1.003	0.993	1.014
0.45	61.50	0.09551	0.00174	1.003	1.002	1.010	0.993	1.001
	69.00	0.09504	0.00176	1.000	1.001	1.009	0.995	1.001
	77.50	0.09406	0.00196	1.000	1.001	1.009	0.997	1.002
	87.00	0.09313	0.00208	0.999	1.000	1.008	0.998	1.002
	98.00	0.09540	0.00204	1.001	1.000	1.007	0.998	1.003
	112.00	0.09308	0.00198	1.001	0.999	1.007	0.998	1.004
	130.00	0.08400	0.00196	1.001	0.999	1.006	0.999	1.005
	152.50	0.08701	0.00209	1.002	0.999	1.006	0.998	1.008
	180.00	0.08816	0.00237	1.002	0.998	1.005	0.997	1.012
	212.50	0.08857	0.00428	1.004	0.998	1.005	0.989	1.017
0.55	61.50	0.05157	0.00131	1.010	1.009	1.023	0.994	1.001
	69.00	0.04726	0.00126	1.008	1.007	1.021	0.996	1.001
	77.50	0.04628	0.00138	1.006	1.006	1.018	0.997	1.001
	87.00	0.04699	0.00152	1.003	1.004	1.017	0.998	1.001
	98.00	0.04616	0.00145	1.005	1.003	1.015	0.999	1.002
	112.00	0.04338	0.00139	1.003	1.002	1.013	0.999	1.002
	130.00	0.04460	0.00150	1.002	1.001	1.012	0.999	1.003
	152.50	0.04496	0.00159	1.002	1.000	1.011	0.999	1.005
	180.00	0.03728	0.00157	1.003	0.999	1.009	0.999	1.007
	212.50	0.04341	0.00192	1.004	0.999	1.008	0.998	1.011
	252.50	0.04589	0.00275	1.006	0.998	1.007	0.993	1.016
0.65	61.50	0.02102	0.00072	1.046	1.021	1.045	0.994	1.000
	69.00	0.02065	0.00075	1.035	1.018	1.040	0.996	1.001
	77.50	0.01902	0.00079	1.029	1.015	1.036	0.998	1.001
	87.00	0.01929	0.00088	1.025	1.012	1.032	0.998	1.001
	98.00	0.01997	0.00091	1.024	1.010	1.029	0.999	1.001
	112.00	0.01978	0.00092	1.017	1.008	1.025	0.999	1.002
	130.00	0.01776	0.00093	1.012	1.006	1.022	0.999	1.002
	152.50	0.01639	0.00096	1.011	1.004	1.019	1.000	1.003
	180.00	0.01840	0.00114	1.008	1.002	1.017	1.000	1.005
	212.50	0.01756	0.00124	1.006	1.001	1.015	0.999	1.007
	252.50	0.01652	0.00143	1.008	0.999	1.013	0.999	1.011
0.75	61.50	0.00706	0.00033	1.147	1.043	1.084	0.994	1.000
	69.00	0.00685	0.00035	1.126	1.037	1.075	0.997	1.000
	77.50	0.00635	0.00037	1.108	1.032	1.066	0.998	1.001
	87.00	0.00605	0.00042	1.099	1.027	1.059	0.998	1.001
	98.00	0.00617	0.00043	1.089	1.022	1.052	0.999	1.001
	112.00	0.00617	0.00044	1.078	1.018	1.046	0.999	1.001
	130.00	0.00558	0.00047	1.063	1.014	1.040	1.000	1.002
	152.50	0.00613	0.00053	1.054	1.010	1.034	1.000	1.002
	180.00	0.00618	0.00063	1.041	1.007	1.029	1.000	1.003
	212.50	0.00507	0.00064	1.034	1.004	1.025	1.000	1.005
	252.50	0.00554	0.00078	1.027	1.002	1.022	1.000	1.008

References

1. BCDMS, D. Bollini et al., Nucl.Instr.Meth. 204(1983)333.
2. BCDMS, D. Bollini et al., Phys.Lett. 104B(1981)403.
3. BCDMS, A. Argento et al., Phys.Lett. 120B(1983)245;
   BCDMS, A. Argento et al., Phys.Lett. 140B(1984)142.
4. BCDMS, R. Kopp et al., Z.Phys. C 28(1985) 171;
   W. Lohmann, R. Kopp and R. Voss, CERN 85-03 (CERN Yellow Report).
5. A.A. Akhundov et al., Sov.J.Nucl.Phys. 26(1977) 660;
   D.Yu. Bardin and N.M. Shumeiko, Sov.J.Nucl.Phys. 29(1979) 499;
   A.A. Akhundov et al., Yad.Fiz. 44(1986) 1517;
   A.A. Akhundov et al., Preprint E2-86-104, Dubna, 1986.
6. G. Altarelli and G. Martinelli, Phys.Lett. 76B(1978) 89.
7. EMC, J.-J. Aubert et al., Nucl.Phys. B272 (1986) 158.
8. BFP, P.D. Meyers et al., Phys.Rev. D34(1986) 1265.
9. BCDMS, A.C. Benvenuti et al., CERN-EP/87-101.
10. EMC, J.-J. Aubert et al., Phys.Lett. 123B(1983) 275;
    R.G. Arnold et al., Phys.Rev.Lett. 52(1984) 722;
    BCDMS, G. Bari et al., Phys.Lett. 163B(1985) 282;
    BCDMS, A.C. Benvenuti et al., Phys.Lett. 189B(1987) 483.

Received by Publishing Department
on July 22, 1987.

Бенвенути А.С. и др. E1-87-549

Измерение с высокой статистикой нуклонной структурной функции $F_2(x, Q^2)$ в глубоконеупругом рассеянии мюонов на углероде при высоких Q^2

Представлены результаты изучения нуклонной структурной функции $F_2(x, Q^2)$, измеренные с высокой статистической точностью в глубоконеупругом рассеянии мюонов на углероде в кинематической области $0,25 \le x \le 0,80$ и $Q^2 \ge 25$ ГэВ^2. Анализ базируется на $1,5 \cdot 10^6$ реконструированных событий, накопленных при энергиях пучка 120, 200 и 270 ГэВ. Найденное значение $R = \sigma_L/\sigma_T$ не зависит от x в области $0,25 \le x \le 0,7$ и 40 ГэВ$^2 \le Q^2 \le 200$ ГэВ^2, и его средняя величина $R = 0,015 \pm 0,013$ /стат./ $\pm 0,026$ /сист./.

Работа выполнена в Лаборатории высоких энергий ОИЯИ.

Препринт Объединенного института ядерных исследований. Дубна 1987

Benvenuti A.C. et al. E1-87-549

A High Statistics Measurement of the Nucleon Structure Function $F_2(x, Q^2)$ from Deep Inelastic Muon-Carbon Scattering at High Q^2

We present results from a high statistics study of the nucleon structure function $F_2(x, Q^2)$ measured in deep inelastic scattering of muons on carbon in the kinematic range $0.25 \le x \le 0.80$ and $Q^2 \ge 25$ GeV^2. The analysis is based on $1.5 \cdot 10^6$ reconstructed events recorded at beam energies of 120, 200 and 280 GeV. $R = \sigma_L/\sigma_T$ is found to be independent of x in the range $0.25 \le x \le 0.7$ and 40 GeV$^2 \le Q^2 \le 200$ GeV with a mean value $R = 0.015 \pm 0.013$ (stat.) ± 0.026 (syst.).

The investigation has been performed at the Laboratory of High Energies, JINR.

Preprint of the Joint Institute for Nuclear Research. Dubna 1987